Final Draft
of the original manuscript:

Erdely, P.; Staron, P.; Maawad, E.; Schell, N.; Klose, J.; Clemens, H.; Mayer, S.:

Design and control of microstructure and texture by thermomechanical processing of a multi-phase TiAl alloy

In: Materials and Design (2017) Elsevier

DOI: 10.1016/j.matdes.2017.06.030

Design and control of microstructure and texture by thermomechanical processing of a multi-phase TiAl alloy

Petra Erdely [a,*], Peter Staron [b], Emad Maawad [b], Norbert Schell [b], Joachim Klose [c], Helmut Clemens [d], Svea Mayer [d]

[a] Recipient of a DOC Fellowship of the Austrian Academy of Sciences at the Department of Physical Metallurgy and Materials Testing, Montanuniversität Leoben, Roseggerstr. 12, A-8700 Leoben, Austria; petra.erdely@unileoben.ac.at.

[b] Institute of Materials Research, Helmholtz-Zentrum Geesthacht, Max-Planck-Str. 1, D-21502 Geesthacht, Germany; peter.staron@hzg.de; emad.maawad@hzg.de; norbert.schell@hzg.de.

[c] GfE Fremat GmbH, Lessingstr. 41, D-09599 Freiberg, Germany; joachim.klose@gfe.com.

[d] Department of Physical Metallurgy and Materials Testing, Montanuniversität Leoben, Roseggerstr. 12, A-8700 Leoben, Austria; helmut.clemens@unileoben.ac.at; svea.mayer@unileoben.ac.at.

[*] Corresponding author. Tel.: +43 3842 402 4213; fax: +43 3842 402 4202.

Abstract

Sheets made of intermetallic γ-TiAl based alloys possess promising engineering properties for lightweight high-temperature applications. Due to the complexity of their manufacturing, however, they are still not fully commercialised. Recently, a manufacturing route has been introduced for β-stabilised γ-TiAl based alloys that is effectively abridged compared to the conventional ingot metallurgy route. The present work explores the impact of each proposed processing stage on a β-solidifying, multi-phase Ti-43.5Al-4Nb-1Mo-0.1B (in at.-%) alloy. Texture measurements using synchrotron radiation were conducted and combined with microstructural analyses. The experiments allowed to fundamentally correlate the processing, which included heat treatment steps for balanced mechanical properties, with the evolution of both microstructure and texture. Thereby, the influences of deformation, recovery and recrystallisation, and phase transformations could be identified. The results reveal several options to optimise the material properties within the cost-effective manufacturing route. One option discussed in depth is the layout of the temperature profile in connection with the

exploitation of the prevailing phase transformations. The presented findings are expected to improve the future design of γ-TiAl based sheet manufacturing routes.

Keywords

TiAl; Processing; Sheet; Texture; Microstructure formation; X-ray synchrotron radiation

1. Introduction

Intermetallic γ-TiAl based alloys combine a low density with high strengths at elevated temperatures and good creep properties [1]. As they are furthermore resistant to oxidation and hot gas corrosion up to roughly 750 °C, they readily meet the demands of lightweight high-temperature applications. Indeed, wrought γ-TiAl based alloys have recently entered service as low-pressure turbine blades in aircraft engines [2,3], and as turbocharger wheels and valves in the automotive industry [4–7]. Rolled products, too, show great potential for aerospace applications. For example, they have been implemented as skin material and tested in thermal and acoustic protection systems, gas leading parts, and exhaust nozzles in propulsion systems for hypersonic air- and spacecraft [8–13]. Due to the complex manufacturing, however, γ-TiAl based sheets have not yet been fully commercialised. With the aim of providing applicable advances in this field, the present work explores the sheet manufacturing of 3rd generation β-solidifying γ-TiAl based alloys. These engineering materials offer significant advantages in terms of processing efficiency, while cultivating the prerequisites for the adjustment of balanced and isotropic mechanical properties [14,15].

Generally, γ-TiAl based sheets can be produced via powder metallurgy (PM) [11] or ingot metallurgy (IM) [12]. The specific assets and drawbacks of both routes are balanced in Refs. [9,16]. In terms of processing stages, the PM route comprises the preparation of γ-TiAl alloy powders, hot-isostatic pressing (HIP), and rolling. In contrast to this, the conventional IM route starts with the casting of γ-TiAl alloy ingots. The ingots are subsequently HIPed, homogenised, and forged or extruded prior to hot rolling [9,12,16]. Most γ-TiAl based alloys

do not provide a sufficiently fine-grained and homogeneous casting microstructure due to a peritectic solidification pathway [12,16]. Only an ingot breakdown does entail the necessary refinement of the cast/HIP microstructure, which represents a basic requirement for successful hot rolling [9]. Recently, it has been shown, though, that γ-TiAl based alloys that solidify via the body-centred cubic (bcc) β phase can satisfy these microstructural requirements already in the cast/HIP condition [17–19]. Consequently, the IM route can be effectively abridged for these alloys, facilitating the production and reducing cost.

With a nominal chemical composition of Ti-43.5Al-4Nb-1Mo-0.1B (in at.-%) that comprises the β-stabilising elements Nb and Mo, the β-solidifying TNM alloy ranges among the promising alloy candidates [14,17]. Within the designation "TNM", "T" stands for TiAl, "N" for Nb, and "M" for Mo. At room temperature, the TNM alloy consists of the three ordered phases α_2-Ti_3Al ($D0_{19}$ structure), β_o-TiAl (B2 structure), and γ-TiAl ($L1_0$ structure). Upon heating, the γ phase remains ordered up to its dissolution temperature $T_{\gamma,solv}$. The hexagonal α_2 and cubic β_o phase transform at elevated temperatures into their disordered counterparts α (A3 structure) and β (A2 structure).

Hot rolling of γ-TiAl based alloys is typically conducted in the (α+γ) or, in the case of β-containing alloys, in the (α+β+γ) region. Production conditions for defect-free sheets have been defined in Ref. [20]. They include carefully adjusted rolling speeds and reductions per pass, and the protection of the sheets from oxidation. For the nominal TNM alloy, successful hot rolling has been demonstrated at various temperatures in the ($\alpha+\beta/\beta_o+\gamma$) and (α+β) region [17,21]. In both regions, the stabilised β phase was exploited to improve the material's hot workability [22]. The sheet manufacturing is typically completed by a primary annealing (PA) treatment to relieve residual stresses and flatten the sheets [9,17].

Most structural high-temperature applications require good creep properties combined with sufficient ductility for handling at room temperature [9]. For the adjustment of such balanced mechanical properties in TNM alloys, a two-step heat treatment has been developed [14,23–

26]. The first step usually represents a high-temperature annealing in the (α+β+γ) or the (α+β) region. It is dedicated to the minimisation of the amount of β/β_o phase and the adjustment of the microstructural features of the α/α_2 and γ phase in terms of phase fraction and size. The β/β_o phase fraction is reduced, since the ordered β_o phase would downgrade the material's creep properties at service temperature [14,22]. The second heat treatment step is characterised by a long-term annealing at temperatures slightly above the prospective service temperature. During this treatment, ultra-fine γ lamellae precipitate in α_2 grains that supersaturated during air cooling in the previous step. Due to a modified Hall-Petch relationship with the mean interface spacing as the dominant structural parameter, the hardness and strength of the material increase [24,27].

The mechanical properties of TNM alloys have been investigated in considerable depth for various microstructural conditions [15,23,24,26,28,29]. Especially for sheet material, though, the mechanical properties are also significantly controlled by texture [30–32]. Intermetallic γ-TiAl based alloys have been reported to develop specific texture components during casting, hot rolling, and PA [16,21,33–39]. Some texture components, such as the modified cube component in the γ phase, have in particular been linked to anisotropic mechanical properties in PA sheets [16,32,34]. The modified cube component has been observed for various alloy compositions. However, it has been shown that significant mechanical anisotropies only occur for sufficiently strong cube components, such as observed e.g. in Ti-46.5Al-4Nb/Mn/Cr/Si/B (at.-%) (γ-TAB) and Ti-46.5Al-4Cr/Nb/Ta/B (at.-%) (γ-MET) alloys [11,37,40,41]. Weak cube components, such as occur e.g. in the so-called TNB alloys [1] and which are often coupled with additional deformation texture components, do not render mechanical properties significantly anisotropic [11,37,42,43]. Literature thus suggests that the presence and relative strength of texture components, which in turn set the material's mechanical properties, can be influenced through the chemical composition of the material and its processing.

Deformation, recovery, recrystallisation, and phase transformations affect each alloy differently. In terms of process optimisation, recrystallisation and phase transformations become especially important during heat treatments. However, while an extensive body of literature exists on the microstructures and textures of as-rolled and PA sheets, little attention has so far been devoted to the optimisation of heat treatments regarding the combination of both factors. In conventional hot-rolled γ-TiAl based alloys, no drastic changes have been observed in the γ phase texture upon annealing [12,35]. In two-phase (α+β) Ti-based alloys, however, whose annealing behaviour is coined by phase transformations between the β and α phase, strong transformation textures have been reported [44–46]. The β-stabilised TNM alloy comprises all three phases α/α_2, β/β_o, and γ in significant amounts. Furthermore, the complexity of the multi-phase system allows for various phase transformations in the course of processing. These circumstances motivate a strategic study tracing the evolution of microstructure and texture from the cast/HIP initial material to the heat-treated TNM sheet.

The present work combines sophisticated tools, which are necessary for the analysis of textures in complex multi-phase materials, with state-of-the-art sheet processing. Linking the texture measurements to detailed structural analyses, an understanding of the basic mechanisms, which shape the material's texture and microstructure over the entire processing cycle, is established. For the first time for a TNM alloy, the hot rolling step is considered separately, i.e. uncoupled from the impact of the subsequent primary annealing. Comparing all selected specimen conditions, which include conditions heat-treated for balanced mechanical properties, the further development and stability of the microstructure and texture can be traced. The deliberate manipulation of the underlying mechanisms, whose principles are also applicable to other alloying systems, is the key to the design and optimisation of the material properties.

2. Material and methods

2.1 Material and processing

The starting material was prepared by way of ingot metallurgy by GfE Metalle und Materialien GmbH, Germany [15,17]. Small ingots (slugs) of a nominal chemical composition of Ti-43.5Al-4Nb-1Mo-0.1B (in at.-%) were produced by means of vacuum arc remelting and centrifugal casting into rotating permanent moulds. To close the residual casting porosity, the ingots were subsequently HIPed for 4 hours at 1200 °C and 200 MPa.

The cast/HIP ingots were hot-rolled on lab scale by GfE Fremat, Germany [17]. The hot rolling was conducted in multiple passes including reheating segments as described in Ref. [9]. By setting the nominal furnace temperature to 1250 °C, the hot rolling temperature was placed slightly below $T_{\gamma,solv}$ in the ($\alpha+\beta+\gamma$) region (Fig. 1). The reduction per rolling pass was set to 10 %. After the last rolling pass, the sheets were furnace-cooled (FC) close to industrial processing conditions to avoid thermal stresses. For the investigation of the as-rolled condition, one sheet was air-cooled (AC) to room temperature. To isolate the impact of the temperature profile generated during hot rolling from effects caused by deformation, one cast/HIP sample was heat-treated in a high-temperature furnace RHF 1600 supplied by Carbolite, UK. The temperature profile was laid out as an emulation of the profile experienced by the as-rolled sheet.

The furnace-cooled sheets were subjected to a PA treatment [9,17] in a vacuum furnace for 1 hour at 1100 °C (Fig. 1). After cooling, the sheets were ground to their ultimate sheet thickness of roughly 1 mm. Thereby, the capsule material was removed.

The ground PA sheets were heat-treated in two steps in the RHF 1600 high-temperature furnace (Fig. 1). The high-temperature annealing HT#1 was conducted for 1 hour at 1240 °C and followed by air cooling. The ensuing stabilisation treatment HT#2 comprised a 6-hour isothermal annealing at 850 °C followed by furnace cooling.

2.2 Experimental techniques

The textures of the three main phases α_2, γ, and β_o were determined by means of high-energy X-ray diffraction (HEXRD) using an area detector [42,47,48]. The measurements were conducted at the P07 high-energy materials science (HEMS) beamline of HZG at PETRA III at the Deutsches Elektronen-Synchrotron (DESY), Germany. Cuboid-shaped specimens of a rectangular cross-section of roughly 1 × 1.2 mm^2 and a height of 20 mm were taken from the sheets at various processing stages (Fig. 1). The longitudinal axis of each specimen represented the rolling direction (RD). Mounted on a goniometer, the RD was aligned parallel to the ω rotation axis. During exposure, the specimens were rotated 180° around the ω axis in steps of $\Delta\omega = 5°$. The specimens were measured in transmission geometry with a photon energy of 87 keV (λ = 0.1424 Å) or 100 keV (λ = 0.1239 Å), and a beam cross-section of 0.5 × 0.5 mm^2. A Perkin Elmer XRD 1622 flat panel detector with a pixel matrix of 2048 × 2048 and a pixel size of 200 × 200 μm^2 recorded the diffraction patterns after each rotation step. The sample-detector distance and the instrumental broadening were calibrated using a LaB_6 powder.

For the texture of the α_2 phase, the $(20\bar{2}0)$, $(20\bar{2}1)$, and $(20\bar{2}2)$ diffraction rings were evaluated, for the β_o phase the (110) and (200) rings, and for the γ phase the (001), (002), (200), and (112) rings. The intensity distribution along the selected Debye-Scherrer rings was transformed into pole figures using the in-house software package SABO as described in Ref. [49]. The azimuthal sections of the diffraction patterns were integrated using the software programme Fit2D [50]. Corrections for the changing volume and absorption were included in the calculations. The orientation distribution functions (ODFs) were estimated using the Matlab toolbox for quantitative texture analysis (MTEX) [51]. De la Vallée Poussin kernels of a half width and a resolution of 5° were selected for the calculation [52]. In the present work, all pole figures, which were recalculated from the respective ODFs, are shown as upper

hemisphere stereographic projections with the RD aligned vertically and the transverse direction (TD) horizontally. In this representation, all main textural features are visible.

The phase fractions were evaluated on the basis of the HEXRD patterns collected for texture analysis. To reduce the texture influence, the patterns recorded at different ω positions were averaged. The commercial software package TOPAS supplied by Bruker AXS, United States, was used for the Rietveld analysis.

The microstructural characterisation was conducted by means of scanning electron microscopy (SEM) on a Zeiss EVO 50. In the back-scattered electron (BSE) mode, the β_o phase appears brightest, the γ phase darkest, and the α_2 phase with an intermediate contrast. The metallographic preparation of the specimens followed Ref. [25]. Two specimens were taken from each sheet such that the planes spanned by the RD and normal direction (ND), as well as by the TD and ND, could be investigated.

On the metallographic specimens, the Vickers hardness (HV5) was measured using a universal hardness testing machine M4C 025 G3M supplied by the Emco Test Company, Austria. Due to the limited sheet thicknesses, a force of 49 N was selected to avoid edge effects. Ten measurements on each specimen were evaluated statistically to a 95% confidence level.

3. Results and discussion

3.1 Microstructure evolution

3.1.1 The cast/HIP initial condition

The nominal TNM alloy of a chemical composition of Ti-43.5Al-4Nb-1Mo-0.1B (at.-%) solidifies via the bcc β phase, i.e. according to the pathway L → (L+β) → β → (β+α) → (…) [14]. In contrast to peritectically solidifying γ-TiAl based alloys, its casting microstructure is fine-grained and homogeneous [14,53,54]. In the cast/HIP condition, the microstructure primarily consists of lamellar α_2/γ colonies of sizes roughly below 50 µm (Fig. 2a). The

colonies are pervaded by a small fraction of precipitated β_o phase, and surrounded by globular or plate-like γ, α_2, and β_o grains (Fig. 2b) [15]. Texture measurements using synchrotron radiation [55] and neutrons [56] have proved the absence of a significant casting texture in the γ and α_2 phase of the TNM alloy. These phases usually form the majority constituents of the TNM microstructure (Table 1). In accordance with Ref. [9], the microstructural features of the cast/HIP TNM alloy fulfil the preconditions for hot rolling, comprising a satisfying microstructural homogeneity, a homogeneous distribution of the alloying elements, and a weak texture [17,53]. The deliberate stabilisation of the β/β_o phase (Table 1) additionally enhances the material's processing capability [22].

3.1.2 Microstructural transformation through hot rolling and primary annealing

The deformation behaviour of γ-TiAl based alloys is largely determined by the selected temperature range [57–59]. Depending on the activated deformation mechanisms and phase transformation paths, various microstructures and textures can be created. Hot rolling in the $(\alpha+\beta+\gamma)$ region slightly below $T_{\gamma,solv}$ has recently been found to offer particularly promising features for the adjustment of balanced mechanical properties [21]. They include the strongest microstructural breakdown in combination with the weakest textures. In the present work, this hot rolling temperature range was, thus, selected as the basis for the TNM sheet manufacturing. Figures 3a and 3b show the microstructure of a specimen hot-rolled in numerous passes including reheating segments. At temperatures slightly below $T_{\gamma,solv}$, the α phase represents the majority microstructural constituent, while the softer β and ordered γ phase are present in minor amounts (Fig. 1) [14]. The amount of γ phase is periodically minimised during the reheating segments in the furnace, and increases again as a result of the inevitable cooling in the lab mill [60]. In the as-rolled condition, which was air-cooled upon the last rolling pass, the microstructure of the TNM alloy primarily consists of lamellar α_2/γ colonies of sizes distinctly below 20 µm. These colonies are surrounded by smaller γ and β_o

grains (Figs. 3a and 3b). The β_o regions appear flattened along both RD and TD, whereas the γ grains still assume a globular shape.

Within the lamellar α_2/γ colonies, the γ lamellae appear rather coarse. Their alignment, as indicated in Figs. 3a' and 3b', is not random but determined by texture and will be discussed in detail in section 3.2.1. Here it should only be noted that a view along the TD (Fig. 3a') reveals a preferred alignment of the lamellae profiles parallel to the RD including a certain tilt. Viewed along the RD (Fig. 3b'), vertical lamellar arrangements can additionally be found.

Due to the straight-lined shape of the lamellae and the fact that the α phase fraction during hot rolling exceeded the now present 35 m.-% (compare Fig. 1 and Table 1), the γ lamellae must have formed upon cooling after the last rolling pass [37]. Their precipitation was promoted by the strong driving force connected with the supersaturation of the α/α_2 grains, and the decelerated heat loss through the capsule material [61]. For further considerations, thus, two populations of γ grains are taken into account; one globular population that was already largely present before air cooling, and one lamellar population that precipitated during cooling within the α/α_2 grains according to the Blackburn orientation relationship [62].

Compared to the cast/HIP condition (Fig. 2), the as-rolled microstructure is substantially refined. This fact, combined with the effects of deformation and changes in the phase fractions, is also reflected in the increased HV5 hardness values. The complete breakdown of the initial grain structure, specifically of prior coarse-lamellar α_2/γ colonies, points to recrystallisation as the primary mechanism for the microstructural refinement [37]. The large number of rolling passes, as well as the numerous reheating segments, also support this assumption [59,60]. To ascertain the observation, one cast/HIP specimen was heat-treated in a high-temperature furnace to identify the impact of the oscillating temperature profile experienced by the material during hot rolling. After cooling, the microstructure of this specimen consists of large α_2 grains, which are surrounded by a continuous seam of β_o phase (Fig. 3c). Coarse γ lamellae, which are present besides some globular γ grains, indicate the

incomplete disintegration of the α_2/γ colonies of the cast/HIP condition. The comparison of the as-rolled specimen (Figs. 3a and 3b) with the one solely heat-treated (Fig. 3c) proves that the microstructural refinement is primarily due to recrystallisation. It cannot be attributed exclusively to the prevailing phase transformations.

The PA step is typically conducted on hot-rolled and furnace-cooled material [17]. As the material approaches thermodynamic equilibrium at 1100 °C, the amounts of γ and β_o phase further increase at the expense of α_2 (Table 1). The dominating increase in γ phase is effected by different mechanisms. First, existing globular γ grains may grow. Secondly, novel globular γ grains may nucleate at various sites within the material, not necessarily exhibiting an orientation relationship with the parent phase [63]. Thirdly, but most importantly, novel γ lamellae precipitate within the α_2 grains and grow and spherodise along with the lamellae already present in the as-rolled condition. The increase in the amount of β_o phase is effected by the growth of already existing β_o grains, as well as by the precipitation of β_o within the lamellar α_2/γ colonies. In sum, a fine-grained microstructure is created, which comprises globular features and a large number of small, disintegrating lamellar α_2/γ colonies (Fig. 4a).

3.1.3 Effect of the two-step heat treatment

The PA sheet was subjected to a two-step heat treatment for balanced mechanical properties [14,24,26]. The first heat treatment step (HT#1) was conducted for 1 hour at 1240 °C in the ($\alpha+\beta+\gamma$) region (Fig. 1). During the isothermal segment, the fraction of α phase increased significantly, while the amount of β phase was successfully minimised (Table 1). As the air cooling was conducted after the removal of the capsule material on altogether thinner sheets, the precipitation of γ lamellae within the supersaturating α/α_2 grains could largely be prevented. At room temperature, the microstructure of condition HT#1, thus, consists of supersaturated α_2 and globular γ and β_o grains (Fig. 4b). The amount of globular γ and β_o can be adjusted through the choice of annealing temperature. Temperatures near $T_{\gamma,solv}$ are preferred, as in this range the β phase fraction passes through a local minimum that is

characteristic of TNM alloys (Fig. 1) [14]. This minimum is capitalised in the course of the heat treatments, as the kinetics of the dissolution of the β phase are sufficiently fast [14,24,26]. Compared to the conditions as-rolled and PA, the microstructure of HT#1 appears slightly coarsened, whereas compared to the initial cast/HIP state the overall microstructural refinement has been retained. The hardness has slightly decreased compared to the PA condition, and the anisotropy expressed by differing values measured in TD and RD is more pronounced. The apparent increase in anisotropy is linked to the increased amount of α_2 phase, which exhibits a hcp crystal structure and a relatively strong texture (see section 3.2.1).

The second heat treatment step (HT#2) represented a long-term annealing at 850 °C followed by furnace cooling. During this treatment, the γ phase fraction increased considerably, while the fraction of β_o remained roughly at the same low level (Table 1). In Fig. 4c the increase in γ phase can be discerned from some γ platelets that formed in the β_o phase. The largest contribution to the phase fraction increase, however, stems from ultra-fine γ lamellae that precipitated in the supersaturated α_2 grains. As described in Refs. [24,26], lamellae formed during this heat treatment step might not be resolved in SEM images. For an isothermal annealing at 850 °C, their average lamellar spacing was found to be roughly 13 nm [24]. However, comparing the hardness of condition HT#1 with that of HT#2, the impact of the lamellae can be observed through a modified Hall-Petch relationship. Starting from the boundaries of the lamellar α_2/γ colonies, the onset of cellular reaction can be observed as reported in Ref. [64].

3.2 Evolution of texture

In Table 2, the texture index J_{ODF} and the entropy S_{ODF} of the calculated ODFs are summarised for each processing stage and for all three phases α_2, γ and β_o. The given values indicate the texture strength (J_{ODF}) and the deviation from a uniform ODF (S_{ODF}) [65]. In the case of a uniform ODF $J_{ODF} = 1$ and $S_{ODF} = 0$, while for a unimodal ODF $J_{ODF} = +\infty$ and S_{ODF} is given by a minimum negative value. In general, all textures created in the nominal

TNM alloy in the course of the presented sheet manufacturing can be classified as weak (Table 2). Distinct textures related to deformation, recrystallisation, and phase transformations are formed, though, which can be deliberately influenced through the choice of the processing parameters.

3.2.1 The α/α_2 phase

In the as-rolled condition, the texture of the α_2 phase consists of both a basal and a transverse texture component [66,67] (Fig. 5). The basal component has been reported to occur in hot-rolled Ti and Ti-based alloys [66–71]. It is characterised by the alignment of the c-axis of the hcp unit cell with the ND of the sheet. In the as-rolled TNM alloy, more specifically a <0001> basal fibre is formed that entails the orientation girdle visible in the $\{10\bar{1}0\}$ pole figure. In accordance with Ref. [39], it is slightly split and tilted towards RD. Additionally, a $<10\bar{1}0>$ fibre with a random orientation girdle along TD–TD in the (0001) pole figure is visible. Besides the dominating basal texture component, a $\{11\bar{2}0\}<0001>$ transverse texture component is present in the as-rolled condition. In (α+β) Ti-based and γ-TiAl alloys, this component is created during hot rolling only in the presence of a second phase, such as β or γ [38,66]. It is defined by the alignment of the c-axis of the hcp unit cell with the TD of the sheet [72]. The orientation of the related prism planes can be identified from the $\{10\bar{1}0\}$ pole figure. Thus, the transverse texture component shows a significant maximum in the ODF for Euler angle ϕ_2=30°, while for the basal component no dependency on ϕ_2 is observed.

The results of the texture measurements agree with the previous microstructural observations (see section 3.1.2). Due to the precipitation of γ lamellae according to the Blackburn orientation relationship $(0001)_{\alpha_2} \| \{111\}_{\gamma}$ and $<11\bar{2}0>_{\alpha_2} \| [1\bar{1}0]_{\gamma}$ [62], the orientation of the $(0001)_{\alpha_2}$ and $\{111\}_{\gamma}$ planes can be analysed from the SEM images. In both Figs. 3a’ and 3b’, horizontally aligned lamellae profiles correspond to an ideal basal texture

component. The actual alignment is not exactly horizontal but varies corresponding to the splitting and tilting of the basal texture component towards RD [39]. Vertical lamellae profiles cannot be observed in Fig. 3a', as in the plane spanned by the RD and ND lamellae that pertain to the transverse texture component are ideally cut parallel to the $(0001)_{\alpha_2}$ and $\{111\}_{\gamma}$ planes. In Fig. 3b', however, which represents the plane spanned by the TD and ND, the hcp grains are cut perpendicularly to the c-axes, which are themselves ideally aligned horizontally. As a result, vertical lamellae profiles are observed for the transverse texture component.

In the hexagonal lattice, slip on prism planes is more easily activated than slip on basal planes due to the higher packing density of the former. Yet, prism planes provide only two independent slip systems [57]. Basal glide offers two additional independent slip systems. Still, pure α does not meet the von-Mises criterion of five independent slip systems for homogeneous plastic deformation, as pyramidal glide as the third option results from of a combination of prism and basal components. In the nominal TNM alloy, however, two processes still ensure a homogeneous and crack-free deformation when hot-rolled with a majority of α phase.

First, the deliberately stabilised, softer β phase accommodates a large part of the deformation, and, thus, supports the predominant activation of soft slip systems, such as prismatic slip, in the neighbouring α phase. The validity of this assumption is proven by the existence of elongated, strongly deformed β grains in the as-rolled condition (Figs. 3a and 3b), as well as by the presence of the transverse texture component in the α_2 phase (Fig. 5). This texture component has been distinctly linked to the predominant activity of soft slip systems by Dunst and Mecking [66], who studied the hot rolling behaviour of two-phase Ti-based alloys at various α/β ratios in the (α+β) region.

The second mechanism is given by the recrystallisation of the α phase itself. Supported by the numerous reheating segments between the rolling passes, local stress concentrations can

be minimised through the movement of grain boundaries. The results of the recrystallisation are apparent from Fig. 3. In contrast to cubic materials, however, hexagonal materials do not always show changes in texture upon recrystallisation [38,44]. Especially when a fraction of second phase is present in the material, as is the case in the nominal TNM alloy, the hot rolling texture tends to be preserved [72,73]. As furthermore no texture components are inherited by the α_2 phase, whose phase fraction only decreases during cooling, all texture components in Fig. 5 can be attributed to the actual hot deformation. It should be noted, though, that the absolute strength of the various components may still be influenced through all processes.

During PA, the fraction of α_2 phase decreases further in favour of the γ and β_o phase (Table 1). Due to the structural rearrangements, the texture of the α_2 phase appears more diffuse (Fig. 5) [39]. Additionally, the overall texture strength has decreased (Table 2). In this regard, however, it should be pointed out that the texture strength in the as-rolled condition might have been overestimated due to slight asymmetries in the pole figures. Asymmetries of this kind easily occur during lab rolling due to shear stresses or differences in the rotational speeds of the rolls. In the PA condition, especially the basal texture component has decreased in intensity. Furthermore, it appears more distinctly split towards RD and more symmetric. A similar splitting of the basal component, which increases during annealing, has also been reported in Ref. [39]. Yet, the basic character of the α_2 phase texture remains unchanged.

Eventually, the PA sheets were subjected to a two-step heat treatment. The first heat treatment step HT#1 at 1240 °C led to a strong increase in the amount of α_2 phase (Table 1). During the presented sheet manufacturing route, this processing step poses the only opportunity of texture inheritance by the α_2 phase. The absence of novel poles within the pole figures in condition HT#1 (Fig. 5), however, leads to the conclusion that the amount of α_2 phase can only have increased through the growth of existing α_2 grains connected with the dissolution of γ and β_o grains, which had previously precipitated from α_2 within short

diffusion paths. Due to the slight grain coarsening during the heat treatment, which is observed in all phases, the overall texture strength expressed by J_{ODF} has increased slightly (Table 2). During HT#2, which represents an annealing step at 850 °C, ultrafine γ lamellae precipitate within the supersaturated α_2 grains. The texture of the α_2 phase itself remains stable.

In sum, the texture of the α_2 phase is defined predominantly by the hot rolling step. The presence and amount of other, softer phases, which depend on the selected hot rolling temperature, determine the relative strength of the basal and transverse texture component [21,66]. During recrystallisation, the generated hot rolling texture remains qualitatively stable. Texture inheritance by the α_2 phase by means of phase transformations is, within the presented manufacturing sequence, only possible during HT#1, in which the α/α_2 phase fraction significantly increases. In the present case, however, novel poles are not observed in the respective set of pole figures. The stability of the α_2 phase texture, especially of the basal component, agrees with the observations by Suwas and Ray [44] for (α+β) Ti-based alloys. The simultaneous decrease in sharpness and increase in width of the basal component is in accordance with Refs. [12,44,74].

3.2.2 The γ phase

Figure 6 illustrates the texture evolution of the γ phase through the (100), (001), and {111} pole figures. Due to the tetragonal distortion of the $L1_0$-structured γ phase (c/a = 1.01), the (100) and (001) planes have to be considered individually. Accordingly, the ideal texture components as reported for hot-rolled or recrystallised face-centred cubic (fcc) materials [75,76] appear split in the γ phase [33,38,39]. In Fig. 6, these ideal components are shown superimposed onto the respective pole figures. In this regard it should be mentioned, though, that the observed textures are in fact rather composed of fibres that link the discrete ideal components as discussed in Ref. [40]. For the γ phase, common fibres include the α1, α2, β1, and β2 fibres. The α fibres typically link Brass to Goss components, i.e. α1 fibres link

B1 to G1 in the centre of the (001) pole figure, and α2 fibres link B2 to G2 in the vicinity of the RD. The β1 fibres characteristically run along B1, S1, Cu1, S1, and B1, and thus close the inner circle in the pole figures, while the β2 fibres comprise the Ms1, S3, Cu2, S2, and B2 components.

Hot rolling in the (α+β+γ) region and subsequent air cooling lead to the formation of two separate texture components (Fig. 6). First, {011}<2$\bar{1}$1> B1 and {110}<$\bar{1}$12> B2 Brass components can be observed in the pole figures. They appear linked by weak β2 fibres. Additionally, α1 fibres can be observed, while β1and α2 fibres are hardly discernible. Brass components are deformation texture components characteristic of fcc metals [75,76]. They have been found in sheets made of γ-TiAl based alloys during the early stages of hot rolling, i.e. after only few rolling passes [40], or when the recrystallisation of the γ phase was suppressed by oil quenching [38] or hindered by the addition of Nb and carbide-forming C [37]. Secondly, a texture component is discernible in the pole figures in Fig. 6 that is not described by any of the ideal deformation or recrystallisation texture components. It is characterised by a <111> fibre parallel to the ND of the sheet, which is split and slightly tilted towards RD.

Hot rolling in the lab mill provokes periodic changes in the γ phase fraction. The inevitable cooling of the sheet in the mill results in an increase in the amount of γ phase, while the γ phase fraction decreases again during the reheating segments between the rolling passes [60]. As the nominal furnace temperature lies slightly below $T_{\gamma,solv}$, reheating leads to an almost complete dissolution of γ phase. Consequently, the deformation texture is largely deleted after each rolling pass. Recrystallisation can potentially occur in the few grains left. The texture, which is observed in the as-rolled condition, stems primarily from the last rolling pass and, most importantly, from phase transformations that took place during air cooling.

During air cooling after the last rolling pass, the amount of γ phase increased considerably. Most significantly, γ lamellae precipitated in supersaturating α/α_2 grains. Thus, the γ phase

inherited the hot rolling texture from the α/α_2 phase according to the Blackburn orientation relationship [62]. Stark et al. [39] showed that the origin of Brass and Goss components can be crystallographically ascribed to the $\alpha/\alpha_2 \rightarrow \gamma$ phase transformation in TiAl alloys. While the Brass B2 component is derived from the ideal transverse component of the α_2 phase, the Goss G2 component correlates with a broadened transverse component. In the present case, the transverse component is not strongly broadened, favouring the Brass over the Goss texture components in the inheritance to the γ phase.

The validity of the Blackburn orientation relationship is proved by the congruency of the $(0001)_{\alpha_2}$and $\{111\}_\gamma$ planes in the respective pole figures (Figs. 5 and 6). The congruency advances even further, as it reveals the relationship not only between the α_2 transverse texture and γ Brass components, but also between the α_2 basal texture and the γ <111> fibre texture as suggested by Brokmeier et al. [37]. Additional poles in the $\{111\}_\gamma$ pole figure are attributed to the multiplicity of $\{111\}_\gamma$ planes compared to the $(0001)_{\alpha_2}$ basal planes, and the angular relationships. Thus, the γ phase exhibits, in the as-rolled condition, primarily transformation texture components inherited from the α/α_2 phase.

PA provokes a further increase of 13 m.-% in the γ phase fraction. The microstructural features become increasingly globular, and lamellar α_2/γ colonies start to degrade. During these processes, the texture of the γ phase becomes weaker and more random, as further γ grains may also nucleate with random orientation (Table 2, Fig. 6) [39]. The close to uniform ODF (S_{ODF} = -0.05, Table 2) introduces uncertainties that account for the apparent anisotropy in the pole figures [76,77]. As a result of this kind of weak texture and randomly oriented grains as the main microstructural constituents, some texture components may not be clearly visible in the pole figures.

During HT#1, the γ phase fraction significantly decreases (Table 1). A population of globular γ grains remains in the microstructure, along with few broad γ lamellae, which could

have precipitated upon cooling, or have been only partly dissolved during the isothermal segment at 1240 °C (Fig. 4). The texture in condition HT#1 can be described as a modified cube texture [16,34,38], combined with α2 and β2 fibres (Fig. 6). Due to the crystallographic tetragonality of the γ phase, the cube texture is split into three variants, i.e. it is modified from the original cube texture [16,40]. The [001] c-axes of the unit cells are aligned parallel to the TD of the sheets, while the [100] a-axes are preferentially aligned along the RD, as well as the ND. The modified cube component has typically been linked to recrystallisation in hot-rolled γ-TiAl based alloys [34,38,40,75]. However, it has also been suggested to originate from the occupation of favourable orientations during hot working and remain stable during hot rolling [37].

In the present work, a modified cube component could not be visibly accumulated during hot rolling due to the cyclic dissolution of the γ phase. However, the grains pertaining to the globular γ phase population, which was observed in the as-rolled condition besides the fraction of γ lamellae (section 3.1.2), are liable to have undergone deformation and may also have already recrystallised. This small fraction of grains remained furthermore stable during PA. During HT#1, the γ phase fraction decreased strongly, but the decrease was primarily realised by the dissolution of γ lamellae (Fig. 4) in accordance with Ref. [37]. Thus, the pole figures in the HT#1 condition represent essentially the texture of the globular γ phase population.

During HT#2, the amount of γ phase increases by a rough absolute value of 50 m.-%. Thus, 72 % of the γ phase are generated through phase transformations either within the β_o or the α_2 phase (Table 1). The vast majority of γ phase precipitates from the supersaturated α_2 grains, and inherits their rolling texture. Consequently, the pole figures in condition HT#2 exhibit only traces of the texture components present in condition HT#1, while Brass B1 and B2 components and a split and tilted <111> fibre are most distinct. As detailed for the as-rolled condition, these components are attributed to the $\alpha_2 \rightarrow \gamma$ phase transformation.

In sum, the texture evolution in the γ phase is sensitive to the choice of processing parameters during sheet manufacturing. Complex textures are created, which contain deformation, recrystallisation, as well as phase transformation components. As large fractions of γ phase transform in the course of the presented processing route, transformation textures most distinctly shape the resulting pole figures. Regarding the multi-step heat treatment, especially the phase transformations between the γ and the α_2 phase influence the texture [61]. The controlled precipitation of γ lamellae within supersaturated α_2 grains allows to maintain a weak texture covering a modified cube component with more uniformly distributed transformation texture components.

3.2.3 The β/β_o phase

During the hot rolling of the cast/HIP TNM alloy, a hot rolling texture characteristic of bcc metals [78,79] is generated in the β phase. It consists of a {111}<$\bar{1}\bar{1}$2> inverse Brass and a {112}<1$\bar{1}$0> texture component (Fig. 7). Additionally, a {001}<110> rotated cube component is present in the as-rolled condition. This component can be attributed to recrystallisation [78].

With regard to γ-TiAl based alloys, Stark [74] suggested the texture of the β/β_o phase to be developed during the early stages of hot rolling and preserved during reheating and annealing. Due to the favourable deformability of the β phase in combination with the high stacking fault energy inherent to the bcc lattice, the tendency towards recovery is strong. As opposed to recrystallisation, recovery does not alter the microstructure or the texture. Furthermore, a strong recovery reduces the driving force for recrystallisation. Recrystallisation components can, thus, occur in the pole figures, but they do not occur exclusively [74]. These observations are in accordance with the findings in the present work (Fig. 7).

PA leads to the nucleation of new β_o grains. Additionally, already existing β_o grains grow as the phase fraction of the β_o phase increases by 10 m.-% (Fig. 4, Table 1). Consequently, the texture of β_o phase in the PA condition becomes more diffuse. Furthermore, the so-called ‘ND’ fibre [79] appears more distinctly developed (Fig. 7). In the {110} pole figure, this fibre

manifests itself through the continuous orientation girdle; <111> directions are aligned parallel to the ND of the sheet. It is also a characteristic component of bcc hot rolling textures [79].

During the further heat treatment steps, the texture of the β_o phase remains stable (Fig. 7). Variations in texture strength and entropy, especially as a result of HT#1, are attributed to the coarsening of β_o grains and the simultaneous minimisation of its phase fraction (Table 2). In HT#2, additional orientations generated by the precipitation of β_o phase in the course of the cellular reaction account for the weaker and more diffuse texture. In sum, the texture of the β_o phase is a weak hot rolling texture characteristic of bcc metals. It tends to be preserved during sheet processing and exhibits only minor changes in texture strength and entropy due to phase transformations.

4. Conclusions

Sheets made of γ-TiAl based alloys increasingly attract attention because of their promising properties for lightweight high-temperature applications. The present work focuses on the sheet manufacturing from a β-stabilised, multi-phase Ti-43.5Al-4Nb-1Mo-0.1B (in at.-%) alloy. Texture measurements conducted at a synchrotron radiation source were combined with microstructural analyses to elucidate the mechanisms that impact both microstructure and texture during various processing stages. The following conclusions can be drawn:

1. During hot rolling, the α_2 phase develops a hot rolling texture consisting of a basal and a transverse texture component. Further processing below $T_{\gamma,solv}$ renders the texture continually more diffuse and weak. However, it remains qualitatively stable.
2. The texture of the γ phase is defined by two mechanisms: deformation and subsequent recrystallisation, and phase transformations. The recrystallisation of γ grains that are deformed during hot rolling leads to the formation of a modified

cube texture. This texture, however, only becomes apparent from the pole figures after the high-temperature annealing step. Only in this condition, the recrystallised grains constitute the majority of the γ phase fraction. A larger influence on the γ phase texture is claimed by the $\alpha/\alpha_2 \rightarrow \gamma$ transformation, as the selected temperature profile enforces the transformation of large phase fractions. The phase transformation is mostly effected through the precipitation of γ lamellae from supersaturated α_2 grains according to the Blackburn orientation relationship. The resulting texture contains multiple components and appears consequently weak.

3. The texture of the β_o phase is determined in the hot rolling step and appears stable during all processing stages.
4. The qualitative stability and continuous weakening of all textures during processing adds a significant robustness to the discussed technological sheet manufacturing routine.

Acknowledgements

The authors thank Dr. Volker Güther, GfE Metalle und Materialien GmbH, and Christiane Rothe, GfE Fremat, for providing the TNM sample material. The support of the DESY management and user office is gratefully acknowledged. We appreciate the commitment of the HZG beamline staff who contributed greatly to the success of the experiments performed. In particular, the authors thank Dr. Andreas Stark for his support at the beamline. Many thanks are given to Dr. Wolfram Schillinger and Dr. Arno Bartels for fruitful discussions.

References

[1] F. Appel, J.D.H. Paul, M. Oehring, Gamma titanium aluminide alloys - Science and technology, Wiley-VCH Verlag & Co. KGaA, Weinheim, Germany, 2011.

[2] B.P. Bewlay, S. Nag, A. Suzuki, M.J. Weimer, TiAl alloys in commercial aircraft engines, Mater. High Temp. 33 (2016) 549–559. doi:10.1080/09603409.2016.1183068.

[3] U. Habel, F. Heutling, D. Helm, C. Kunze, W. Smarsly, G. Das, et al., Forged intermetallic γ-TiAl based alloy low pressure turbine blade in geared turbofan, in: V. Venkatesh, A.L.

Pilchak, J.E. Allison, A. Sreeramamurthy, R. Boyer, J. Christodoulou, et al. (Eds.), 13th World Conf. Titan., Wiley, USA, San Diego, California, 2016: pp. 1223–1227. doi:10.1002/9781119296126.

[4] T. Noda, Application of cast gamma TiAl for automobiles, Intermetallics 6 (1998) 709–713. doi:10.1016/S0966-9795(98)00060-0.

[5] T. Tetsui, Development of a TiAl turbocharger for passenger vehicles, Mater. Sci. Eng. A 329–331 (2002) 582–588. doi:10.1016/S0921-5093(01)01584-2.

[6] H. Baur, D.B. Wortberg, H. Clemens, Titanium aluminides for automotive applications, in: Y.-W. Kim, H. Clemens, A.H. Rosenberger (Eds.), Gamma Titan. Alum. 2003, The Minerals, Metals and Materials Society, Warrendale, PA, USA, 2003: pp. 23–31.

[7] MWRacing, Products/Titanium Aluminide Valves, Catalogue. (2017). http://www.mwracing.eu/Products/Titanium-Aluminide-Valves.aspx (accessed March 1, 2017).

[8] S.L. Draper, D. Krause, B. Lerch, I.E. Locci, B. Doehnert, R. Nigam, et al., Development and evaluation of TiAl sheet structures for hypersonic applications, Mater. Sci. Eng. A 464 (2007) 330–342. doi:10.1016/j.msea.2007.02.020.

[9] H. Clemens, Intermetallic γ-TiAl based alloy sheet materials - processing and mechanical properties, Z. Metallkd. 86 (1995) 814–822.

[10] G. Das, H. Kestler, H. Clemens, P.A. Bartolotta, Sheet gamma TiAl: status and opportunities, JOM 4 (2004) 42–45. doi:10.1007/s11837-004-0251-y.

[11] R. Gerling, H. Clemens, F.P. Schimansky, Powder metallurgical processing of intermetallic gamma titanium aluminides, Adv. Eng. Mater. 6 (2004) 23–38. doi:10.1002/adem.200310559.

[12] C. Koeppe, A. Bartels, H. Clemens, P. Schretter, W. Glatz, Optimizing the properties of TiAl sheet material for application in heat protection shields or propulsion systems, Mater. Sci. Eng. A 201 (1995) 182–193. doi:10.1016/0921-5093(94)09754-2.

[13] H. Clemens, S. Mayer, Intermetallic titanium aluminides in aerospace applications - processing, microstructure and properties, Mater. High Temp. 33 (2016) 560–570. doi:10.1080/09603409.2016.1163792.

[14] H. Clemens, W. Wallgram, S. Kremmer, V. Güther, A. Otto, A. Bartels, Design of novel β-solidifying TiAl alloys with adjustable β/B2-phase fraction and excellent hot-workability, Adv. Eng. Mater. 10 (2008) 707–713. doi:10.1002/adem.200800164.

[15] H. Clemens, S. Mayer, Design, processing, microstructure, properties, and applications of advanced intermetallic TiAl alloys, Adv. Eng. Mater. 15 (2013) 191–215. doi:10.1002/adem.201200231.

[16] A. Bartels, H. Kestler, H. Clemens, Deformation behavior of differently processed γ-titanium aluminides, Mater. Sci. Eng. A 331 (2002) 153–162. doi:10.1016/S0921-5093(01)01552-0.

[17] M. Achtermann, V. Güther, J. Klose, C. Rothe, I. Eulitz, Manufacturing and properties of TiAl TNM sheet materials, in: GAT 2013, Toulouse, 2013.

[18] Y.F. Liang, Z.Z. Shen, H. Wang, L.Q. Zhang, X.J. Xu, Y. Xu, et al., Manufacturing and properties of high Nb-TiAl sheet materials, in: Y.-W. Kim, W. Smarsly, J. Lin, D.M. Dimiduk, F. Appel (Eds.), Gamma Titan. Alum. 2014, John Wiley & Sons, Inc., Hoboken, New Jersey, 2014: pp. 83–86.

[19] Z.Z. Shen, J.P. Lin, Y.F. Liang, L.Q. Zhang, S.L. Shang, Z.K. Liu, A novel hot pack rolling of high Nb–TiAl sheet from cast ingot, Intermetallics 67 (2015) 19–25. doi:10.1016/j.intermet.2015.07.009.

[20] H. Clemens, P. Schretter, K. Wurzwallner, A. Bartels, C. Koeppe, Forging and Rolling of Ti48Al2Cr on industrial scale, in: R. Darolia, J.J. Lewandowski, C.T. Liu, P.L. Martin, D.B. Miracle, M.V. Nathal (Eds.), Struct. Intermet. 1993, Warrendale, PA, USA, 1993: p. 205.

[21] P. Erdely, P. Staron, E. Maawad, N. Schell, J. Klose, S. Mayer, et al., Effect of hot rolling and

primary annealing on texture and microstructure of a β-stabilised γ-TiAl based alloy, Acta Mater. 126 (2017) 145–153. doi:10.1016/j.actamat.2016.12.056.

[22] T. Tetsui, K. Shindo, S. Kobayashi, M. Takeyama, A newly developed hot worked TiAl alloy for blades and structural components, Scr. Mater. 47 (2002) 399–403. doi:10.1016/S1359-6462(02)00158-6.

[23] W. Wallgram, T. Schmölzer, L. Cha, G. Das, V. Güther, H. Clemens, Technology and mechanical properties of advanced γ-TiAl based alloys, Int. J. Mater. Res. 100 (2009) 1021–1030. doi:10.3139/146.110154.

[24] L. Cha, H. Clemens, G. Dehm, Microstructure evolution and mechanical properties of an intermetallic Ti-43.5Al-4Nb-1Mo-0.1B alloy after ageing below the eutectoid temperature, Int. J. Mater. Res. 102 (2011) 703–708. doi:10.3139/146.110526.

[25] M. Schloffer, T. Schmoelzer, S. Mayer, E. Schwaighofer, G. Hawranek, F.-P. Schimansky, et al., The characterisation of a powder metallurgically manufactured TNM^{TM} titanium aluminide alloy using complimentary quantitative methods, Pract. Metallogr. 48 (2011) 594–604. doi:10.3139/147.110138.

[26] E. Schwaighofer, H. Clemens, S. Mayer, J. Lindemann, J. Klose, W. Smarsly, et al., Microstructural design and mechanical properties of a cast and heat-treated intermetallic multi-phase γ-TiAl based alloy, Intermetallics 44 (2014) 128–140. doi:10.1016/j.intermet.2013.09.010.

[27] L. Cha, C. Scheu, H. Clemens, H.F. Chladil, G. Dehm, R. Gerling, et al., Nanometer-scaled lamellar microstructures in Ti-45Al-7.5Nb-(0; 0.5)C alloys and their influence on hardness, Intermetallics 16 (2008) 868–875. doi:10.1016/j.intermet.2008.03.009.

[28] L.M. Droessler, T. Schmoelzer, W. Wallgram, L. Cha, G. Das, H. Clemens, Microstructure and tensile ductility of a Ti-43Al-4Nb-1Mo-0.1B alloy, in: Mater. Res. Soc. Symp. Proc., MRS Warrendale, 2009: p. 121.

[29] T. Voisin, J.-P. Monchoux, M. Hantcherli, S. Mayer, H. Clemens, A. Couret, Microstructures and mechanical properties of a multi-phase β-solidifying TiAl alloy densified by spark plasma sintering, Acta Mater. 73 (2014) 107–115. doi:10.1016/j.actamat.2014.03.058.

[30] D.G. Morris, M.A. Morris-Muñoz, The importance of textures for determining the mechanical behaviour of intermetallics, Intermetallics 8 (2000) 997–1003. doi:10.1016/s0966-9795(00)00033-9.

[31] H. Mecking, C. Hartig, Effects of processing on texture, microstructure and related properties of TiAl alloys, in: Y.-W. Kim, R. Wagner, M. Yamaguchi (Eds.), Gamma Titan. Alum. 1995, The Minerals, Metals and Materials Society (TMS), 1995: pp. 525–538.

[32] W. Schillinger, B. Lorenzen, A. Bartels, Anisotropic mechanical behavior of textured γ-TiAl caused by the directionality of twinning, Mater. Sci. Eng. A 329–331 (2002) 644–648. doi:10.1016/S0921-5093(01)01662-8.

[33] H. Fukutomi, C. Hartig, H. Mecking, Change of microstructure in a TiAl intermetallic compound during high temperature deformation, Z. Metallkd. 81 (1990) 272–277.

[34] C. Hartig, X.F. Fang, H. Mecking, M. Dahms, Textures and plastic anisotropy in γ-TiAl, Acta Metall. Mater. 40 (1992) 1883–1894. doi:10.1016/0956-7151(92)90175-E.

[35] C. Hartig, H. Fukutomi, H. Mecking, K. Aoki, Texture and microstructure of Ti-49%Al after dynamic recrystallization and annealing, ISIJ Int. 33 (1993) 313–320.

[36] A. Bartels, W. Schillinger, Micromechanical mechanism of texture formation in γ-TiAl, Intermetallics 9 (2001) 883–889. doi:10.1016/S0966-9795(01)00086-3.

[37] H.-G. Brokmeier, M. Oehring, U. Lorenz, F. Appel, H. Clemens, Neutron diffraction study of texture development during hot working of different gamma-titanium aluminide alloys, Metall. Mater. Trans. A 35 (2004) 3563–3579. doi:10.1007/s11661-004-0193-6.

[38] W. Schillinger, A. Bartels, R. Gerling, F.-P. Schimansky, H. Clemens, Texture evolution of the

γ- and the α/α_2-phase during hot rolling of γ-TiAl based alloys, Intermetallics 14 (2006) 336–347. doi:10.1016/j.intermet.2005.07.002.

[39] A. Stark, A. Bartels, R. Gerling, F.-P. Schimansky, H. Clemens, Microstructure and texture formation during hot rolling of niobium-rich γ TiAl alloys with different carbon contents, Adv. Eng. Mater. 8 (2006) 1101–1108. doi:10.1002/adem.200600127.

[40] A. Bartels, W. Schillinger, G. Grassl, H. Clemens, Texture formation in γ-TiAl sheets, in: Y.-W. Kim, H. Clemens, A.H. Rosenberger (Eds.), Gamma Titan. Alum. 2003, TMS, Warrendale, PA, USA, 2003: pp. 275–286.

[41] W. Schillinger, H. Clemens, G. Dehm, A. Bartels, Microstructural stability and creep behavior of a lamellar γ-TiAl based alloy with extremely fine lamellar spacing, Intermetallics 10 (2002) 459–466. doi:10.1016/S0966-9795(02)00021-3.

[42] K.-D. Liss, A. Bartels, A. Schreyer, H. Clemens, High-energy X-rays: A tool for advanced bulk investigations in materials science and physics, Textures Microstruct. 35 (2003) 219–252. doi:10.1080/07303300310001634952.

[43] S. Bystrzanowski, A. Bartels, H. Clemens, R. Gerling, F.-P. Schimansky, G. Dehm, et al., Creep behaviour and related high temperature microstructural stability of Ti-46Al-9Nb sheet material, Intermetallics 13 (2005) 515–524. doi:10.1016/j.intermet.2004.09.001.

[44] S. Suwas, R.K. Ray, Stability of rolling texture during heat treatment in a two-phase Ti_3Al base intermetallic alloy, Acta Mater. 47 (1999) 4599–4614. doi:10.1016/S1359-6454(99)00328-6.

[45] G.C. Obasi, R.J. Moat, D.G. Leo Prakash, W. Kockelmann, J. Quinta Da Fonseca, M. Preuss, In situ neutron diffraction study of texture evolution and variant selection during the α → β → α phase transformation in Ti-6Al-4V, Acta Mater. 60 (2012) 7169–7182. doi:10.1016/j.actamat.2012.09.026.

[46] I. Lonardelli, N. Gey, H.-R. Wenk, M. Humbert, S.C. Vogel, L. Lutterotti, In situ observation of texture evolution during α → β and β → α phase transformations in titanium alloys investigated by neutron diffraction, Acta Mater. 55 (2007) 5718–5727. doi:10.1016/j.actamat.2007.06.017.

[47] L. Wcislak, J. Schneider, T. Tschentscher, H. Klein, H.J. Bunge, Hard X-ray texture measurements with an on-line image plate detector, Nucl. Instruments Methods Phys. Res. Sect. A Accel. Spectrometers, Detect. Assoc. Equip. 467–468 (2001) 1257–1260. doi:10.1016/S0168-9002(01)00649-0.

[48] H.-R. Wenk, S. Grigull, Synchrotron texture analysis with area detectors, J. Appl. Crystallogr. 36 (2003) 1040–1049. doi:10.1107/S0021889803010136.

[49] S. Yi, Investigation on the deformation behavior and the texture evolution in magnesium wrought alloy AZ31, Ph.D thesis, Technische Universität Clausthal, 2005.

[50] A.P. Hammersley, S.O. Svensson, M. Hanfland, A.N. Fitch, D. Hausermann, Two-dimensional detector software: From real detector to idealised image or two-theta scan, High Press. Res. 14 (1996) 235–248. doi:10.1080/08957959608201408.

[51] R. Hielscher, H. Schaeben, A novel pole figure inversion method: Specification of the MTEX algorithm, J. Appl. Crystallogr. 41 (2008) 1024–1037. doi:10.1107/S0021889808030112.

[52] H. Schaeben, A simple standard orientation density function: The hyperspherical de la Vallée Poussin kernel, Phys. Status Solidi. 200 (1997) 367–376. doi:10.1002/1521-3951(199704)200:2<367::AID-PSSB367>3.0.CO;2-I.

[53] V. Küstner, M. Oehring, A. Chatterjee, V. Güther, H.-G. Brokmeier, H. Clemens, et al., An investigation of microstructure formation during solidification of gamma titanium aluminide alloys, in: Y.-W. Kim, H. Clemens, A.H. Rosenberger (Eds.), Gamma Titan. Alum. 2003, The Minerals, Metals and Materials Society (TMS), Warrendale, PA, USA, 2003: pp. 89–96.

[54] Y. Jin, J.N. Wang, J. Yang, Y. Wang, Microstructure refinement of cast TiAl alloys by β solidification, Scr. Mater. 51 (2004) 113–117. doi:10.1016/j.scriptamat.2004.03.044.

[55] E. Schwaighofer, B. Rashkova, H. Clemens, A. Stark, S. Mayer, Effect of carbon addition on solidification behavior, phase evolution and creep properties of an intermetallic β-stabilized γ-TiAl based alloy, Intermetallics 46 (2014) 173–184. doi:10.1016/j.intermet.2013.11.011.

[56] H. Clemens, H.F. Chladil, W. Wallgram, G.A. Zickler, R. Gerling, K.-D. Liss, et al., In and ex situ investigations of the β-phase in a Nb and Mo containing γ-TiAl based alloy, Intermetallics 16 (2008) 827–833. doi:10.1016/j.intermet.2008.03.008.

[57] F. Appel, M. Oehring, J.D.H. Paul, C. Klinkenberg, T. Carneiro, Physical aspects of hot-working gamma-based titanium aluminides, Intermetallics 12 (2004) 791–802. doi:10.1016/j.intermet.2004.02.042.

[58] H.Z. Niu, Y.F. Chen, Y.S. Zhang, J.W. Lu, W. Zhang, P.X. Zhang, Phase transformation and dynamic recrystallization behavior of a β-solidifying γ-TiAl alloy and its wrought microstructure control, Mater. Des. 90 (2016) 196–203. doi:10.1016/j.matdes.2015.10.133.

[59] S.Z. Zhang, C.J. Zhang, Z.X. Du, Z.P. Hou, P. Lin, F.T. Kong, et al., Deformation behavior of high Nb containing TiAl based alloy in α+γ two phase field region, Mater. Des. 90 (2016) 225–229. doi:10.1016/j.matdes.2015.10.080.

[60] H. Zhou, F. Kong, K. Wu, X. Wang, Y. Chen, Hot pack rolling nearly lamellar Ti-44Al-8Nb-(W, B, Y) alloy with different rolling reductions: Lamellar colonies evolution and tensile properties, Mater. Des. 121 (2017) 202–212. doi:10.1016/j.matdes.2017.02.053.

[61] Y. Zong, D. Wen, Z. Liu, D. Shan, γ-Phase transformation, dynamic recrystallization and texture of a forged TiAl-based alloy based on plane strain compression at elevated temperature, Mater. Des. 91 (2016) 321–330. doi:10.1016/j.matdes.2015.11.120.

[62] M.J. Blackburn, Some aspects of phase transformations in titanium alloys, in: R.I. Jaffee, N.E. Promisel (Eds.), Sci. Technol. Appl. Titan., Plenum Press, New York, 1970: pp. 639–642.

[63] H.K.D.H. Bhadeshia, Problems in the calculation of transformation texture in steels, ISIJ Int. 50 (2010) 1517–1522. doi:10.2355/isijinternational.50.1517.

[64] M. Kastenhuber, B. Rashkova, H. Clemens, S. Mayer, Enhancement of creep properties and microstructural stability of intermetallic β-solidifying γ-TiAl based alloys, Intermetallics 63 (2015) 19–26. doi:10.1016/j.intermet.2015.03.017.

[65] D. Mainprice, F. Bachmann, R. Hielscher, H. Schaeben, Descriptive tools for the analysis of texture projects with large datasets using MTEX: strength, symmetry and components, Geol. Soc. London, Spec. Publ. 409 (2014) 251–271. doi:10.1144/SP409.8.

[66] D. Dunst, H. Mecking, Analysis of experimental and theoretical rolling textures of two-phase titanium alloys, Z. Metallkd. 87 (1996) 498–507.

[67] H. Inagaki, Hot rolling textures in high-strength Ti alloys, Z. Metallkd. 81 (1990) 433–445.

[68] H. Inagaki, Hot rolling textures in Ti, Z. Metallkd. 81 (1990) 282–292.

[69] S. Suwas, R.K. Ray, A.K. Singh, S. Bhargava, Evolution of hot rolling textures in a two-phase (α_2+β) Ti_3Al base alloy, Acta Mater. 47 (1999) 4585–4598. doi:10.1016/S1359-6454(99)00327-4.

[70] A.K. Singh, R. Schwarzer, Texture and anisotropy of mechanical properties in titanium and its alloys, Z. Metallkd. 91 (2000) 702–716.

[71] S.K. Sahoo, R.K. Sabat, S. Sahni, S. Suwas, Texture and microstructure evolution of commercially pure titanium during hot rolling: Role of strain-paths, Mater. Des. 91 (2016) 58–71. doi:10.1016/j.matdes.2015.11.073.

[72] Y.N. Wang, J.C. Huang, Texture analysis in hexagonal materials, Mater. Chem. Phys. 81 (2003) 11–26. doi:10.1016/S0254-0584(03)00168-8.

[73] R.D. Doherty, D.A. Hughes, F.J. Humphreys, J.J. Jonas, D. Juul Jensen, M.E. Kassner, et al., Current issues in recrystallization: A review, Mater. Sci. Eng. A 238 (1997) 2019–274. doi:10.1016/S1369-7021(98)80046-1.

[74] A. Stark, Textur- und Gefügeentwicklung bei der thermomechanischen Umformung Nb-reicher γ-TiAl-Basislegierungen, Shaker Verlag, 2010.

[75] H.J. McQueen, H. Mecking, Hot rolling deformation and recrystallization textures in fcc metals, Z. Metallkd. 78 (1987) 387–396.

[76] J. Hirsch, K. Lücke, Mechanism of deformation and development of rolling textures in polycrystalline f.c.c. metals - I. Description of rolling texture development in homogeneous CuZn alloys, Acta Metall. 36 (1988) 2863–2882. doi:10.1016/0001-6160(88)90172-1.

[77] A. Creuziger, K. Syed, T. Gnäupel-Herold, Measurement of uncertainty in orientation distribution function calculations, Scr. Mater. 72–73 (2014) 55–58. doi:10.1016/j.scriptamat.2013.10.017.

[78] D. Raabe, K. Lücke, Rolling and annealing textures of bcc metals, in: Proc. 10th Int. Conf. Textures Mater. Part 1, Materials Science Forum, Clausthal, Germany, 1994: pp. 597–610. doi:10.4028/www.scientific.net/MSF.157-162.597.

[79] S. Mercier, L.S. Tóth, A. Molinari, Modelling of texture development and deformation mechanisms in a Ti20V alloy using a self consistent polycrystal approach, Textures Microstruct. 25 (1995) 45–61. doi:10.1155/TSM.25.45.

Figure captions

Fig. 1: Schematic representation of the TNM sheet manufacturing. Dots on the timeline indicate the stages at which specimens were taken for examination. The as-rolled specimen was air-cooled (AC) to retrieve information on the actual hot rolling process. Specimens PA, HT#1, and HT#2 were furnace-cooled (FC) after hot rolling to minimise thermal stresses. On the left, a corresponding detail of the TNM phase fraction diagram is given as drawn from data in Ref. [26]. The shared temperature scaling allows to retrace the equilibrium phase fractions approached during the respective processing steps.

Fig. 2: Microstructure of the cast/HIP TNM alloy. In (**a**) the HV5 hardness is given in the top right corner. The main microstructural features are labelled at a higher magnification in (**b**). In the SEM-BSE mode, the β_o phase appears brightest, the γ phase darkest, and the α_2 phase with an intermediate contrast.

Fig. 3: SEM images highlighting the microstructural refinement of the cast/HIP TNM alloy through hot rolling in the ($\alpha+\beta+\gamma$) region. Figures (**a**, **b**) show the as-rolled condition. Fig. (**c**) represents a specimen that was subjected to a temperature profile similar to that of the multi-step hot rolling procedure. In Figs. (**a**) and (**c**), the main microstructural features are indicated. Arrows labelled ‘RD’, ‘TD’, and ‘ND’ give the orientation of the investigated cross-sections with respect to the coordinate system of the sheet (**a**, **b**) or the ingot (**c**). The orientations of the lamellar colonies after hot rolling, such as indicated in the magnified details (**a’**) and (**b’**), are a direct consequence of the created texture (see section 3.2.1).

Fig. 4: Primary-annealed (**a**) and heat-treated (**b**, **c**) microstructures of the nominal TNM alloy. The microstructural features elaborated in the text are indicated by labelled marks. Arrows labelled ‘RD’, ‘TD’, and ‘ND’ give the orientation of the investigated cross-sections with respect to the coordinate system of the sheets. In the top right corners the corresponding HV5 hardness values are given.

Fig. 5: (0001) and $\{10\bar{1}0\}$ pole figures of the α_2-Ti_3Al phase. Characteristic stages of the TNM sheet manufacturing are shown including ideal basal and transverse texture components as given in Refs. [39,66,72]. The PA condition is considered in depth in Ref. [21]. On the right hand side, the corresponding phase fractions of the α_2 phase are given.

Fig. 6: (100), (001), and {111} pole figures of the γ-TiAl phase. Characteristic stages of the TNM sheet manufacturing are shown including ideal deformation and recrystallisation texture components as given in Refs. [38,39,76]. The PA condition considered in depth in Ref. [21]. On the right hand side, the corresponding phase fractions of the γ phase are given.

Fig. 7: {100} and {110} pole figures of the β_o-TiAl phase. Characteristic stages of TNM sheet manufacturing are shown, including ideal hot rolling and recrystallisation texture components as given in Refs. [78,79]. The PA condition considered in depth in Ref. [21]. On the right hand side, the corresponding phase fractions of the β_o phase are given.

Tables

Table 1: Phase fractions (incl. standard deviation SD) at various processing stages as determined by means of HEXRD and Rietveld fitting. For the assessment of the Rietveld analysis, the R-factors R_p and R_{wp} are given. Slightly elevated values correlate with reduced grain statistics due to comparably coarse-grained microstructures.

Specimen	Phase fractions [m.-%] ± SD			R_p	R_{wp}
	α_2 phase	γ phase	β_o phase		
cast/HIP	11.4 ± 0.2	68.5 ± 0.6	20.1 ±0.2	5.56	8.59
as-rolled	34.4 ± 0.4	57.4 ± 0.7	8.2 ±0.2	7.91	10.26
PA	11.8 ± 0.2	70.5 ± 0.9	17.7 ± 0.3	5.77	7.19
HT#1	80.0 ± 2.2	19.0 ± 0.6	1.0 ± 0.1	9.61	11.79
HT#2	29.6 ± 0.9	68.3 ± 1.9	2.1 ± 0.1	9.80	12.27

Table 2: Texture index J_{ODF} and entropy S_{ODF} as calculated from the estimated ODFs.

Specimen	Texture index J_{ODF}			Entropy S_{ODF}		
	α_2 phase	γ phase	β_o phase	α_2 phase	γ phase	β_o phase
as-rolled	3.02	1.25	1.13	-0.70	-0.07	-0.09
PA	1.84	1.11	1.11	-0.36	-0.05	-0.05
HT#1	1.94	1.30	1.64	-0.33	-0.12	-0.30
HT#2	1.90	1.12	1.13	-0.32	-0.05	-0.06

Figures

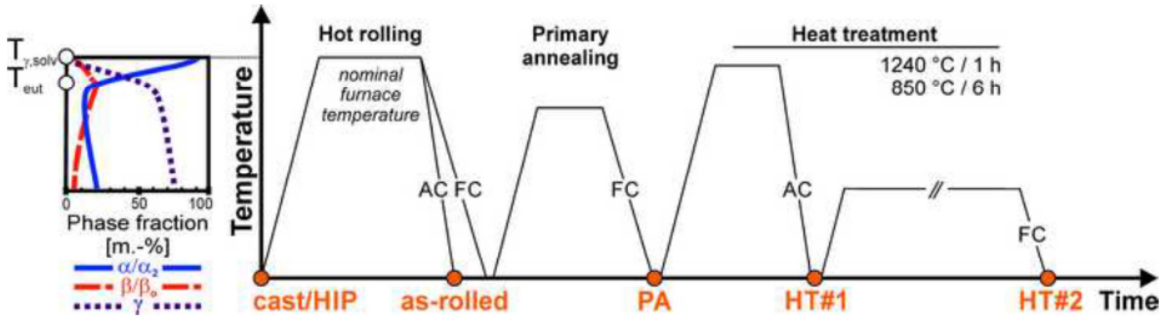

Fig. 1: Schematic representation of the TNM sheet manufacturing. Dots on the timeline indicate the stages at which specimens were taken for examination. The as-rolled specimen was air-cooled (AC) to retrieve information on the actual hot rolling process. Specimens PA, HT#1, and HT#2 were furnace-cooled (FC) after hot rolling to minimise thermal stresses. On the left, a corresponding detail of the TNM phase fraction diagram is given as drawn from data in Ref. [26]. The shared temperature scaling allows to retrace the equilibrium phase fractions approached during the respective processing steps.

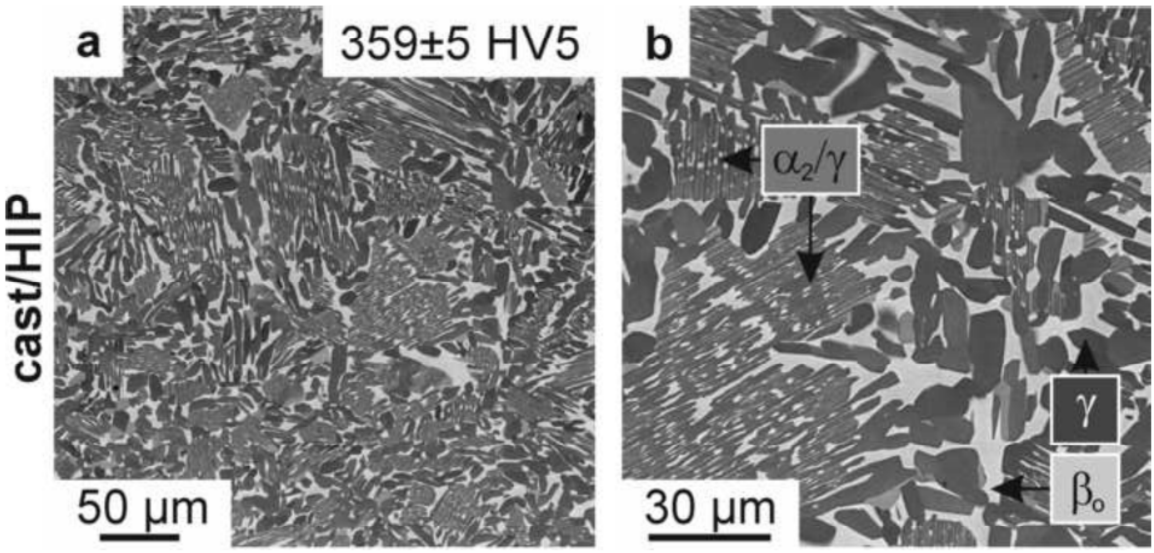

Fig. 2: Microstructure of the cast/HIP TNM alloy. In (**a**) the HV5 hardness is given in the top right corner. The main microstructural features are labelled at a higher magnification in (**b**). In the SEM-BSE mode, the β_o phase appears brightest, the γ phase darkest, and the α_2 phase with an intermediate contrast.

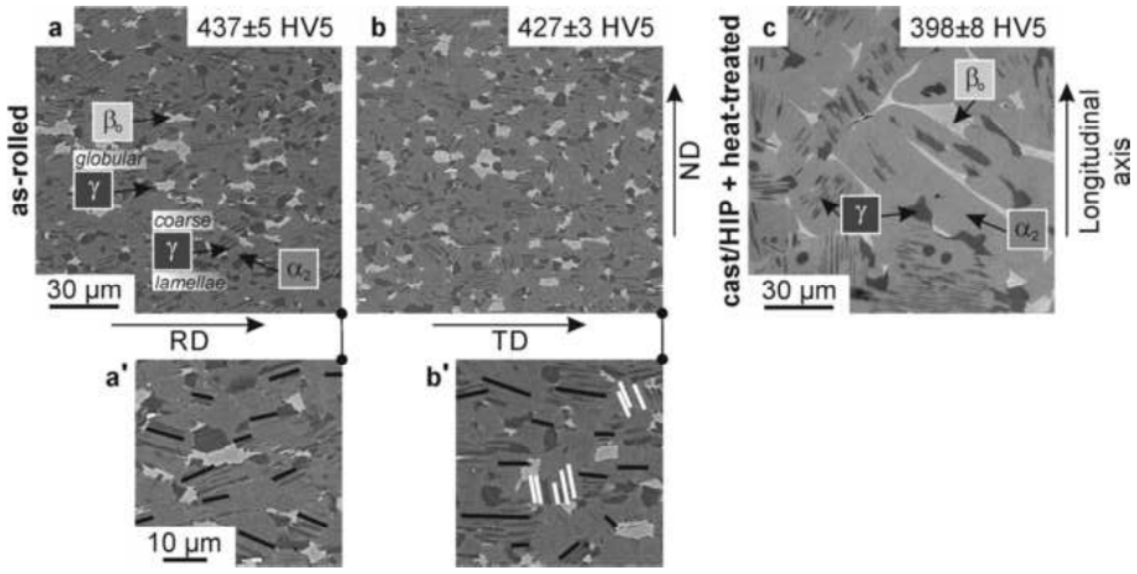

Fig. 3: SEM images highlighting the microstructural refinement of the cast/HIP TNM alloy through hot rolling in the (α+β+γ) region. Figures (**a**, **b**) show the as-rolled condition. Fig. (**c**) represents a specimen that was subjected to a temperature profile similar to that of the multi-step hot rolling procedure. In Figs. (**a**) and (**c**), the main microstructural features are indicated. Arrows labelled 'RD', 'TD', and 'ND' give the orientation of the investigated cross-sections with respect to the coordinate system of the sheet (**a**, **b**) or the ingot (**c**). The orientations of the lamellar colonies after hot rolling, such as indicated in the magnified details (**a'**) and (**b'**), are a direct consequence of the created texture (see section 3.2.1).

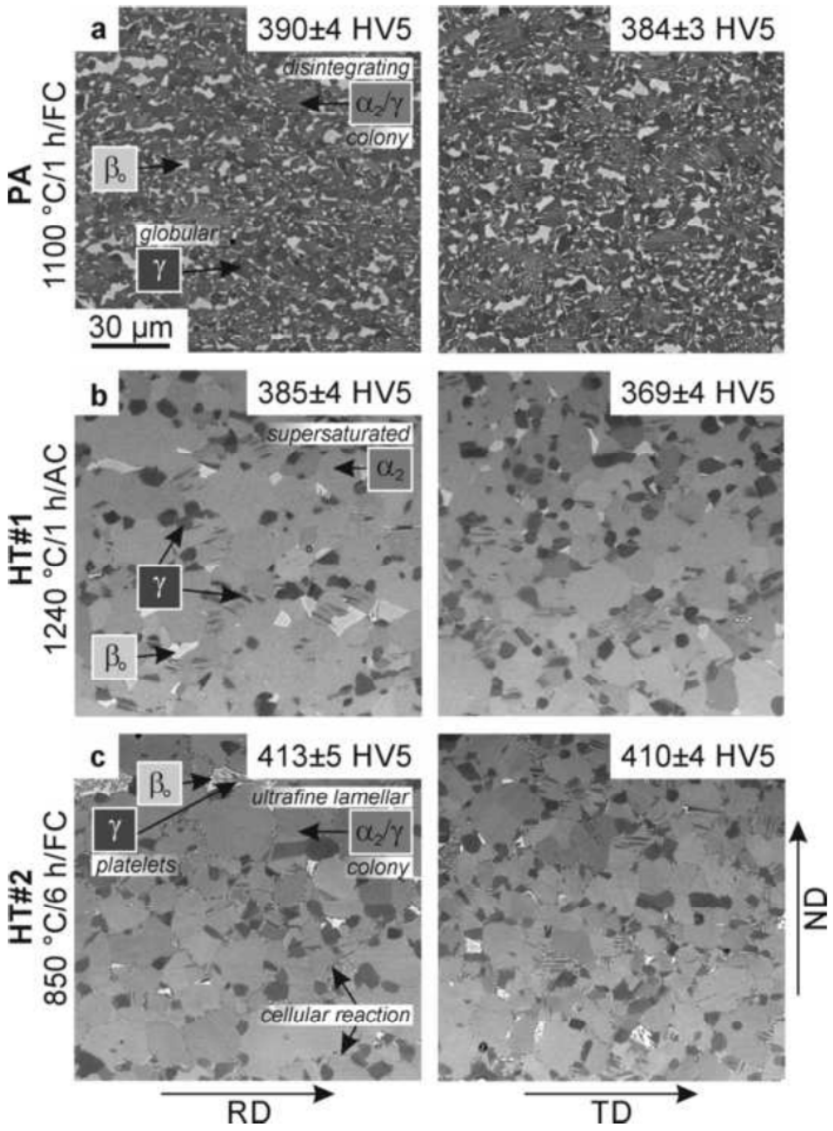

Fig. 4: Primary-annealed (**a**) and heat-treated (**b**, **c**) microstructures of the nominal TNM alloy. The microstructural features elaborated in the text are indicated by labelled marks. Arrows labelled ‘RD’, ‘TD’, and ‘ND’ give the orientation of the investigated cross-sections with respect to the coordinate system of the sheets. In the top right corners the corresponding HV5 hardness values are given.

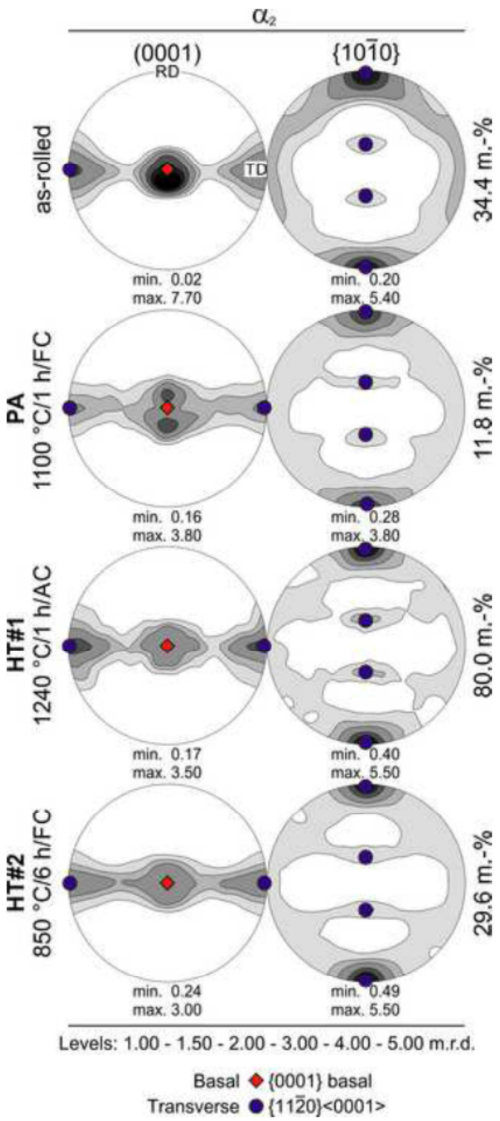

Fig. 5: (0001) and $\{10\bar{1}0\}$ pole figures of the α_2-Ti_3Al phase. Characteristic stages of the TNM sheet manufacturing are shown including ideal basal and transverse texture components as given in Refs. [39,66,72]. The PA condition is considered in depth in Ref. [21]. On the right hand side, the corresponding phase fractions of the α_2 phase are given.

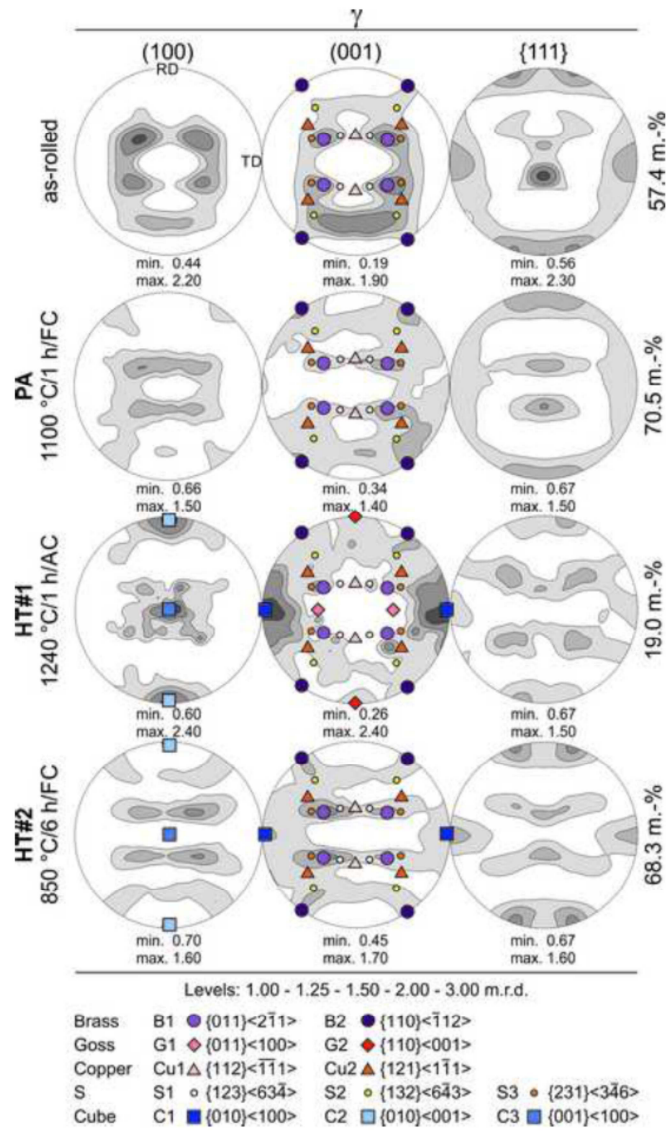

Fig. 6: (100), (001), and {111} pole figures of the γ-TiAl phase. Characteristic stages of the TNM sheet manufacturing are shown including ideal deformation and recrystallisation texture components as given in Refs. [38,39,76]. The PA condition considered in depth in Ref. [21]. On the right hand side, the corresponding phase fractions of the γ phase are given.

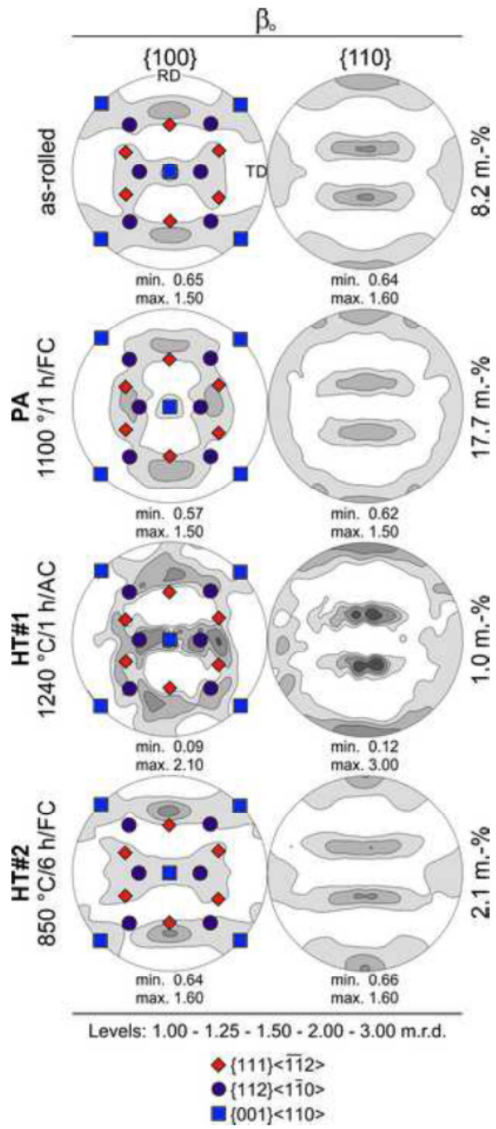

Fig. 7: {100} and {110} pole figures of the β_o-TiAl phase. Characteristic stages of TNM sheet manufacturing are shown, including ideal hot rolling and recrystallisation texture components as given in Refs. [78,79]. The PA condition considered in depth in Ref. [21]. On the right hand side, the corresponding phase fractions of the β_o phase are given.